January 2002

Nontunneling high-order harmonics from ultra-intense laser-driven tightly bound systems

S. X. Hu
University of Nebraska - Lincoln

Anthony F. Starace
University of Nebraska-Lincoln, astarace1@unl.edu

W. Becker
Max-Born-Institut, Max-Born-Strasse 2A, 12489 Berlin, Germany

W. Sandner
Max-Born-Institut, Max-Born-Strasse 2A, 12489 Berlin, Germany

D. B. Milosevic
Max-Born-Institut, Max-Born-Strasse 2A, 12489 Berlin, Germany

Published in *Journal of Physics B: Atomic, Molecular and Optical Physics* 35 (2002), pp. 627–650.
Online at http://stacks.iop.org/JPhysB/35/627

Submitted August 31, 2001; revised December 10, 2001; published January 31, 2002.

Nontunneling high-order harmonics from ultra-intense laser-driven tightly bound systems

S. X. Hu,[1] A. F. Starace,[1] W. Becker,[2,4] W. Sandner,[2,5] and D. B. Milošević [2,3]

[1] Department of Physics and Astronomy, University of Nebraska–Lincoln, 116 Brace Laboratory, Lincoln, NE 68588-0111, USA
[2] Max-Born-Institut, Max-Born-Strasse 2A, 12489 Berlin, Germany
[3] Faculty of Science, University of Sarajevo, Zmaja od Bosne 35, 71000 Sarajevo, Bosnia and Hercegovina
[4] Department of Physics and Astronomy, University of New Mexico, Albuquerque, NM 87131, USA.
[5] Optisches Institut, Technische Universität Berlin, 10623 Berlin, Germany.
Correspondence: email shu@unlnotes.unl.edu & wbecker@mbi-berlin.de

Abstract

High-order harmonic emission is investigated by numerical solution of the weakly relativistic, two-dimensional Schrödinger equation for the case of ultraintense laser-driven tightly bound systems (for example, multiply charged ions such as O^{7+} exposed to laser fields of the order of 10^{18} W cm^{-2} at 248 nm). In contrast to their usual substantial decrease, the low-order harmonics having an energy less than the ionization potential exhibit a high-efficiency (i.e. intense) plateau with a well defined cutoff. The shape of this plateau is found to depend on the shape of the binding potential. A classical "surfing" mechanism for the generation of these harmonics is proposed that does not involve tunneling and that nevertheless explains the observed cutoff. Thus we call them "nontunneling harmonics." The significance of relativistic effects for these harmonics is investigated and found to be small, despite the high laser intensity, because of the absence of tunneling.

1. Introduction and overview

Any nonlinear system that is driven by a monochromatic field will respond at harmonic frequencies of the driving field. For low driving-field intensity (such that perturbation theory with respect to the system–field coupling is applicable) the harmonic response quickly decreases with increasing harmonic order. For stronger fields, it may stabilize over an extended range of orders before it eventually drops off. Such a "plateau" in the harmonic response is characteristic of neutral atoms exposed to intense laser fields. Indeed, high-order harmonic generation (HHG) by atoms, molecules, and clusters in intense laser fields has become a very active field of research since its first observation more than 15 years ago; for recent reviews, see [1,

2]. HHG is on the verge of providing versatile table-top sources of intense radiation with a unique temporal structure and for frequencies reaching into the water window [3, 4].

Experiments have preferentially employed Ti:Sa lasers, featuring high intensity and short pulses, and rare-gas targets, which have high ionization potentials. Hence, the theoretical work has concentrated on these also. For these cases, HHG is well described by the three-step or recombination scenario [5, 6]: this assumes that an electron tunnels into the continuum, where its subsequent accelerated motion is driven by the laser field. Depending on the time when it tunnels out, it may eventually collide and recombine with the ionic core, releasing its energy by emission of a single harmonic photon. This model predicts that the plateau terminates at a cutoff energy of $I_p + 3.17U_p$, where U_p denotes the ponderomotive energy $U_p = E^2/4\omega^2$, ω and E are the laser frequency and field amplitude, and I_p is the ionization potential of the atom. (The ponderomotive energy is the cycle average of the laser-induced energy of oscillation of the electron.) The harmonic spectrum then has a very typical appearance: over the first few harmonics, the intensities decrease substantially; at a harmonic order roughly equal to I_p/ω, the recombination mechanism begins to become effective in forming the plateau up to the above-mentioned cutoff, after which there is a rapid drop of HHG intensity below detectability. This tunneling–recombination mechanism has so dominated the scene that one may be inclined to assume that it is a precondition for plateau-like HHG.

In this paper, as the medium for HHG we shall consider multiply charged ions, specifically those having the same binding energy as O^{7+}. Such ions may be produced in a number of ways (for a recent review, see [7]; see also [8]). Plans to combine intense lasers beams with intense ion beams are already well under way [9]. Also, free-electron lasers using undulators may use the merged beam technique, which is already well established in synchrotron studies of ions [10]. Additionally, we note that theorists have proposed using ensembles of ions for harmonic generation in the femtosecond regime [11].

We assume that the multiply charged ions are exposed to ultra-strong fields [12], with intensities in the range of 10^{18} W cm^{-2}, so that if an electron were to move only under the influence of the laser field, it would obey relativistic kinematics. The pertinent ionization potentials easily reach hundreds of electron volts. As a consequence, the "low-energy" part of the harmonic spectrum defined by harmonic orders below I_p/ω, which for neutral atoms only includes a few harmonics, may now extend over hundreds of harmonics. For neutral atoms, this part is too short to develop any evident structure. For multiply charged ions, this low-energy part of the HHG spectrum is extensive and, as we shall show, exhibits its own characteristic structure.

We expect that HHG in this case will be quite different from the standard situation, for several reasons. First, tunneling will play a lesser role because the tunneling rate decreases exponentially with Z^3, where Z is the charge of the ionic core; see, for example, the review [13]. Second, any electron that does nevertheless tunnel out will be driven away from the ionic core by the Lorentz force via the magnetic-field component of the applied laser field. Third, for tightly bound systems some intermediate states remain bound when exposed to ultra-intense laser fields, and they might play an important role in HHG. All three of these factors combine to reduce the role of the tunneling–recombination mechanism for the case of multiply charged ion targets in the low-energy part of the HHG spectrum. In addition, we note that the precise shape of the binding potential does not play a very significant role in the standard tunneling–recombination mechanism. Indeed, this is a precondition for the applicability of models such as the Lewenstein model [14] and others [15]. In contrast, we shall show that the shape of the binding potential has an important influence on HHG in the case of multiply charged ions.

We shall investigate HHG arising from irradiation of tightly bound systems with ultra-intense laser fields by numerically solving the weakly relativistic, two-dimensional, time-dependent Schrödinger equation. We shall focus on the effect of the shape of the binding potential on the "low-order" harmonics, that is, those with an order below I_p/ω. We shall explore the transition from a soft-core potential to a Coulomb-like potential. The former, owing to its relatively flat bottom, can be considered as a model for ionized clusters [16], while the Coulombic potential is more realistic for a hydrogen-like multiply charged ion. For the soft-core potential, our calculations reveal the existence of a plateau in the low-order harmonic regime whose appearance is very similar to the standard tunneling–recombination plateau even though its physical origin is completely different. However, when the binding potential becomes narrower and approaches the Coulombic shape of a hydrogen-like ion, the low-order harmonic spectrum changes drastically. The plateau turns into a narrow hump with, however, a smaller plateau still extending from one of its shoulders. The position of the hump is associated with an excited bound state. We formulate a classical model that is able to explain both kinds of plateau and their cutoffs [17]. The mechanism is such that the corresponding harmonics could aptly be called "surfing harmonics." However, we prefer to call them "nontunneling harmonics" because of the absence of tunneling in their generation. The harmonic intensities—both for the plateau characteristic of the soft-core potential and for the hump-shaped plateau characteristic of the hydrogen-like potential—are higher than for HHG in rare gases near saturation by several orders of magnitude. This is not really surprising: standard HHG is related to tunneling, which is a weak process, while the nontunneling harmonics that we consider here are due to the inner atomic dynamics, which affect a much larger part of the wavefunction. We shall also investigate potentials having a shape close to that of a square well and compare the results to HHG by a two-level system. We find that there exist some shared features, such as hyper-Raman lines.

Finally, we shall assess the significance of relativistic effects. In our calculations, we do not invoke the dipole approximation, so that the effect of the magnetic field is fully included. In addition, our calculation also incorporates lowest-order truly relativistic effects of order $1/c$ compared with magnetic-field effects. Even though the laser field that we employ causes a free electron to quiver with a speed of about $0.3c$, the low-order harmonic spectrum, in contrast to the tunneling–recombination plateau, betrays few relativistic effects. Qualitatively most notable is the emission of very-low-order even harmonics due to a magnetic dipole transition. The lowest-order relativistic term leaves virtually no mark in the harmonic spectrum. This may be regarded as further evidence that free excursions of the active electron under the influence of the laser field (that are characteristic of the usual tunneling–recombination description of HHG) do not contribute to low-order harmonics.

We only consider harmonic emission by a single ion. Also, we do not dwell on the practical prospects of providing an ion source with the appropriate density [8]. Whether or not this may ultimately turn out to be feasible, our results confirm that the emission of high-order harmonics and, in particular, the existence of a plateau in this spectrum are very general features of nonlinearly driven systems and by no means restricted to the tunneling– recombination mechanism.

Briefly, the paper is organized as follows: in Section 2 we present our numerical procedure for solving the weakly relativistic Schrödinger equation and introduce the model potentials to which it is applied. In Section 3, we present and discuss nontunneling radiation spectra for these potentials. In particular, we propose a classical mechanism that appears to underlie the formation of the quantum mechanically predicted plateaus. We also investigate the role of excited states and their dc Stark shifts, and assess finally the importance of magnetic-field and relativistic effects. Atomic units are used throughout this paper, unless noted otherwise. In Section 4 we present our conclusions.

2. Models and numerical method

Since the strong-field approximation and the associated Lewenstein model [14, 15] are not applicable for inner-atomic harmonic emission, we solve the time-dependent Schrödinger equation directly, using well known methods [18–20].

2.1. Numerical solution of the weakly relativistic Schrödinger equation

We consider an ultra-intense laser pulse with an intensity of 1.9×10^{18} W cm^{-2} at the KrF laser wavelength of 248 nm. For these parameters, the maximal velocity of a free electron subject to this pulse is about $0.3c$ (with c the speed of light), and the ponderomotive energy is $U_p \approx 0.02mc^2$. This corresponds to the weakly relativistic regime. Therefore, for an electron in the continuum, the magnetic field will be important [21] while truly relativistic effects will still be small. In order to take the action of the magnetic field into account, we have to allow for at least two spatial dimensions. We expand the fully relativistic Hamiltonian so as to include first-order relativistic corrections. Subtracting the rest mass, we have

$$\begin{aligned} H &= \sqrt{(\boldsymbol{p} + \boldsymbol{A}/c)^2 c^2 + c^4} - c^2 + V(x, z) \\ &\simeq V(x, z) + \frac{1}{2}(\boldsymbol{p} + \boldsymbol{A}/c)^2 - \frac{1}{8c^2}(\boldsymbol{p} + \boldsymbol{A}/c)^4, \end{aligned} \tag{1}$$

with $\boldsymbol{p} = (p_x, 0, p_z)$ the operator of the two-dimensional canonical momentum. The laser field is a plane wave linearly polarized along the x direction and propagating in the z direction, as described by the vector potential

$$\boldsymbol{A} = A_x(t, z)\boldsymbol{e}_x = A_0 f(u) \cos \omega u \, \boldsymbol{e}_x . \tag{2}$$

It depends on space and time only via $u = t - z/c$. The pulse-shape function $f(u)$ is normalized to a maximum of $f(u) = 1$; unless stated otherwise, it will be chosen trapezoidal, with a linear turn-on of five cycles and a flat section of ten cycles. For the binding potential $V(x, z)$ we shall consider different forms, as discussed below. For harmonic generation and not too highly charged ions, we can safely neglect the electron's spin [22]. Hence, we shall use the spinless Schrödinger equation with the Hamiltonian (1). We then apply the weakly relativistic extension of the usual split-operator algorithm [18] to study the time-dependent evolution of the system under the irradiation of the external laser pulse. That is, the time evolution of the wavefunction is approximated by

$$\begin{aligned} \Psi(x, z, t + \Delta t) = \exp\left[-\frac{\mathrm{i}}{2}\Delta t f_1(p_x, p_z)\right] \exp\left[-\frac{\mathrm{i}}{2}\Delta t f_3(z, p_x, t)\right] \exp[-\mathrm{i}\Delta t f_2(x, z, t)] \\ \times \exp\left[-\frac{\mathrm{i}}{2}\Delta t f_3(z, p_x, t)\right] \exp\left[-\frac{\mathrm{i}}{2}\Delta t f_1(p_x, p_z)\right] \Psi(x, z, t). \end{aligned} \tag{3}$$

For a free electron, application of p_x or A_x/c to the wavefunction yields terms of the same order of magnitude. The other momentum component p_z, however, is of the order of $p_x A_x/c$. In the approximation (3), we keep terms up to the order of p_x^4 or equivalent. We then have

$$f_1(p_x, p_z) = (p_x^2 + p_z^2)/2 - p_x^4/8c^2, \tag{4}$$

$$f_2(x, z, t) = V(x, z) + A_x(t, z)^2/2c^2 - A_x(t, z)^4/8c^6, \tag{5}$$

$$f_3(z, p_x, t) = p_x A_x(t, z)/c - p_x^3 A_x(t, z)/2c^3 - 3\, p_x^2 Ax(t, z)^2/4c^4 - p_x A_x(t, z)^3/2c^5, \tag{6}$$

where the three functions f_i ($i = 1, 2, 3$) depend on the momentum operator, the position operator, and both the momentum component p_x and the position component z, respectively. In order to compute the action of the operators f_i, we transform, re-

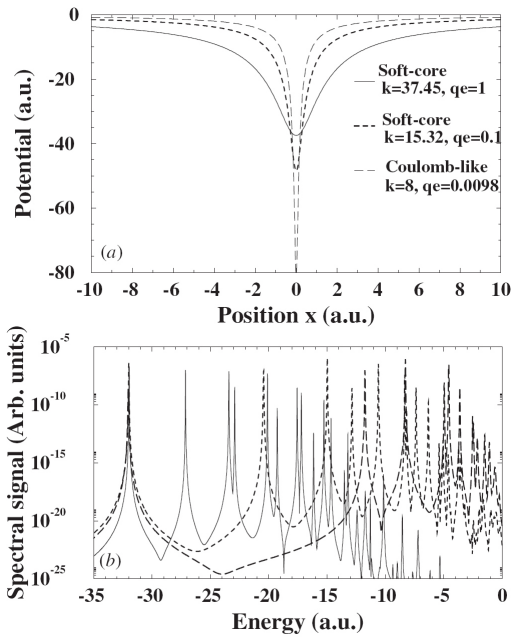

Figure 1. (*a*) The shape of various model potentials $V(x, z)$ (equation (7)) with different parameters k and q_e. (*b*) The corresponding energy levels. Note that for all potentials the ground-state energy is kept constant with a value of −32 au, which equals

spectively, to the representation where f_i is diagonal. That is, for the application of f_1, we transform the wavefunction to momentum space. Next, for the application of f_3, we transform back to position space in z, and further, for application of f_2 we complete the transformation back to position space. Finally, the same steps are carried out again in reverse. Similar techniques have been employed in [23, 24].

2.2. Model potentials

We shall consider various forms of the static binding potential that models the interaction between the outmost electron and the ionic core. One will be the soft-core Coulomb potential [25]

$$V(x, z) = -\frac{k}{\sqrt{q_e + x^2 + z^2}}. \tag{7}$$

Here the parameter k represents the charge of the ionic core. The smoothing parameter q_e eliminates the Coulomb singularity and determines the depth of the potential. In a simulation that involves fewer than three dimensions, the presence of such a parameter is physically reasonable since otherwise the electron would get too close to the core too often. We have employed the so-called "spectral method" [18] in order to calculate the energy spectrum in the absence of the laser field as a function of the parameters k and q_e. In all examples, we have kept the ground-state energy constant at −32 au, which corresponds to the ground state of the hydrogen-like ion O^{7+}. Magnetic-field effects are very small for an electron in this state. Figure 1 shows the shape of the binding potential (7) and the associated energy levels for three different combinations of the parameters k and q_e. For the large value of k = 37.45 and q_e = 1, we get a relatively flat potential with a rather high density of energy levels. Such a soft-core potential may describe an electron in an ionized cluster [16]. When

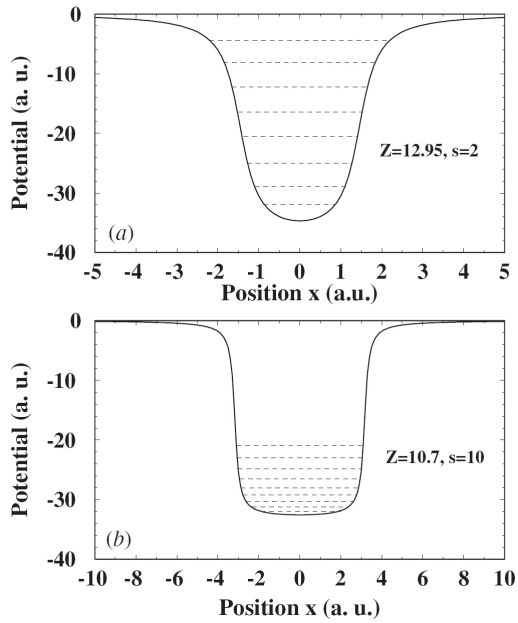

Figure 2. Two model square wells (8) for (***a***) $Z = 12.95$ and $s = 2$, and (***b***) $Z = 10.7$ and $s = 10$. The energy levels are indicated by dashed lines.

we decrease both parameters, the potential develops a more pronounced minimum. At the same time, the separation of the low-lying energy levels increases. The smallest parameters shown, i.e. $k = 8$ and $q_e = 0.0098$, are chosen so that the parameter k is exactly equal to the nuclear charge of the hydrogen-like ion O^{7+}. The parameter q_e now is extremely small, and the potential is very close to that of a pure Coulomb potential. The energy levels approximate a Rydberg series. In general, for hydrogen-like ions described by the potential (7), the smoothing parameter q_e scales as $q_e(\mathrm{H})/Z^2$ (where $q_e(\mathrm{H}) \sim 0.63$ is the value for atomic hydrogen) [25].

For reasonable values of the parameters, the potential (7) has a pronounced minimum. It is interesting to consider a potential where this minimum is replaced by an extended almost flat section, as would be the case in a large-Z positive ion in which the inner shell electrons are averaged over. Since the ideal square well is unsuitable for numerical calculations owing to its discontinuity, we shall consider the potential

$$V(x, z) = Z[\arctan(x^2 + z^2 - s) - \pi/2]. \tag{8}$$

As the parameter s increases, the potential approaches that of a square well of radius $\sqrt{s}$. In Figure 2 we plot two such "square wells" for the parameters $Z = 12.95$ and $s = 2$, as well as $Z = 10.7$ and $s = 10$. They are chosen so that the ground-state energy is −32 au in either case.

Finally, we shall compare the harmonic spectra of the two model potentials (7) and (8) with those generated by a two-level system coupled to the electric field $\boldsymbol{E}(t) = \boldsymbol{E}_0 \sin \omega t$. The two-level system cannot be represented exactly by any local potential in position space. It is described by the Hamiltonian

$$H(t) = \begin{pmatrix} -\omega_0/2 & \Omega_0 \sin \omega t \\ \Omega_0 \sin \omega t & \omega_0/2 \end{pmatrix} \tag{9}$$

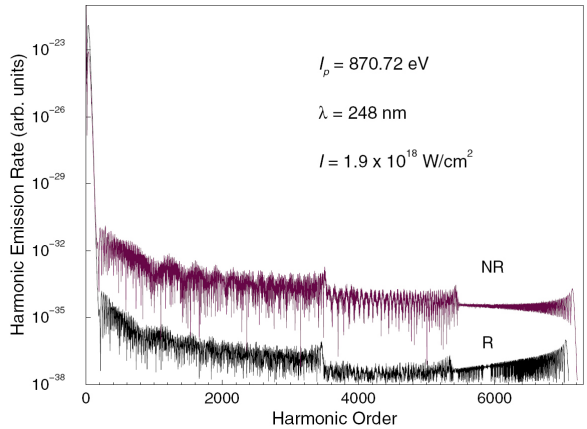

Figure 3. The spectrum of the "tunneling–recombination" harmonics obtained using the Lewenstein (NR) strong-field approximation theory and its relativistic generalization (R) for the hydrogen-like ion model with I_p = 870.72 eV. The laser intensity is 1.9×10^{18} W cm^{-2} and the wavelength is λ = 248 nm.

where

$$\Omega_0 = -\boldsymbol{\mu} \cdot \boldsymbol{E}_0 \tag{10}$$

denotes the Rabi frequency with $\boldsymbol{\mu}$ the electric-dipole transition matrix element between the two states of the system. The system can be represented by two time-dependent coefficients $c_1(t)$ and $c_2(t)$ so that $|\psi(t)\rangle = c_1(t)|1\rangle + c_2(t)|2\rangle$. They satisfy the coupled first-order differential equations

$$\begin{aligned} \mathrm{i}\,\mathrm{d}c_1(t)/\mathrm{d}t &= -\frac{\omega_0}{2}\,c_1(t) + \Omega_0 \sin\omega t\; c_2(t), \\ \mathrm{i}\,\mathrm{d}c_2(t)/\mathrm{d}t &= \frac{\omega_0}{2}\,c_2(t) + \Omega_0 \sin\omega t\; c_1(t). \end{aligned} \tag{11}$$

The time-dependent mean dipole moment can be calculated from $d(t) = \mu[c_1^*(t)c_2(t) + c_1(t)c_2^*(t)]$, which leads to the radiation spectrum via Fourier transformation.

3. Results and discussions

We are concerned with the *low-order* harmonics radiated by strongly bound electrons, whose ionization potential I_p equals many atomic units. By "low" we refer to harmonics with an order of less than I_p/ω. This is the part of the harmonic spectrum where usually, for harmonics produced by atoms or singly charged ions, the harmonic intensities strongly and uniformly decrease with increasing order. "Low-order harmonics" is a relative term: in our example we have $I_p/\omega = 174$. The harmonic spectrum is obtained through Fourier analysis of the mean dipole acceleration or, for the two-level system, the dipole moment of the electron.

3.1. Plateau of nontunneling harmonics

In order to set the stage, we start by showing in Figure 3 the tunneling–recombination harmonic spectrum for a binding energy of −32 au and a laser intensity of 1.9×10^{18} Wcm^{-2}, calculated for the hydrogen-like ion model by using either the nonrelativistic (NR) Lewenstein strong-field approximation [14] or its relativistic generalization (R) [27]. According to the NR theory [26], the plateau cutoff is

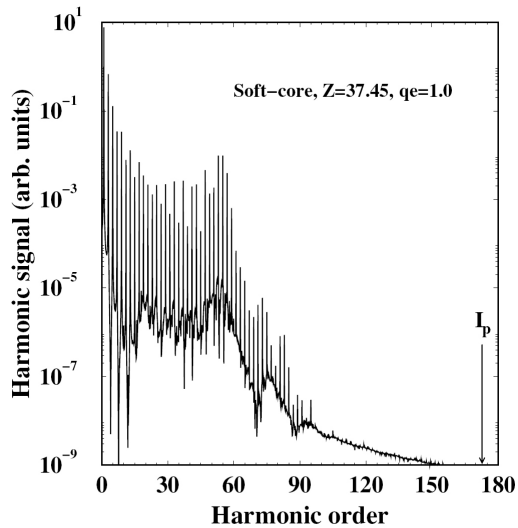

Figure 4. The spectrum of the "nontunneling harmonics" for an electron in the soft-core model potential (7), with $k = 37.45$ and $q_e = 1$, exposed to a laser with an intensity of 1.9×10^{18} Wcm^{-2} and a wavelength $\lambda = 248$ nm. The arrow at the lower right marks the harmonic order having an energy equal to the ionization potential, $I_p = 870.72$ eV.

at $(1.325I_p + 3.173U_p)/\omega = 7155$; the relativistic calculation yields a slightly lower cutoff. The harmonic spectra exhibit the multiplateau structure that is characteristic of the weakly relativistic regime [27]. There is a huge drop by at least ten orders of magnitude from the emission rates of the low-order harmonics (harmonic orders below 100) to the emission rates of the plateau harmonics. Since we are in the weakly relativistic regime, the reason for this difference is not primarily due to relativistic effects, but to the very high value of the ionization potential. However, comparison of the relativistic and the NR spectrum shows that the former is further reduced by three orders of magnitude owing to the $\boldsymbol{v} \times \boldsymbol{B}$ drift. In view of the very low yield of the standard plateau harmonics, in the following we shall concentrate on the low-order harmonics.

The plateaux produced by the Lewenstein model are largely independent of the precise choice of the binding potential. In contrast, the low-order harmonics (which are not reliably modeled by the Lewenstein model) crucially depend on the binding potential. First, we consider the soft-core potential (7) with a large smoothing parameter, that is, $k = 37.45$ and $q_e = 1$. In Figure 4 we present the corresponding harmonic spectrum. The harmonic order $I_p/\omega = 174$, where the tunneling–recombination plateau of Figure 3 begins, is marked by an arrow in the lower right of the figure. The plateau of Figure 4 has largely the appearance of a common tunneling–recombination plateau. It consists entirely of odd harmonics and has a well defined cutoff at about $n = 59$. Its physical origin, however, is completely different. This will be discussed next.

If the extent of the spatial grid used in the numerical solution of the Schrödinger equation is reduced to about ten atomic units, the harmonics displayed in Figure 4 hardly change. This proves that they cannot be due to the standard mechanism where the electron (having tunneled out of the atom) performs an excursion of about $\alpha = E/\omega^2$ (calculated here nonrelativistically), whose value under our conditions is about 500 au. Hence, we conclude that the origin of these harmonics is to be sought in the inner atomic dynamics. We suggest that they are produced when a laser-driven *bound* electronic wavepacket sweeps over the center of the binding potential.

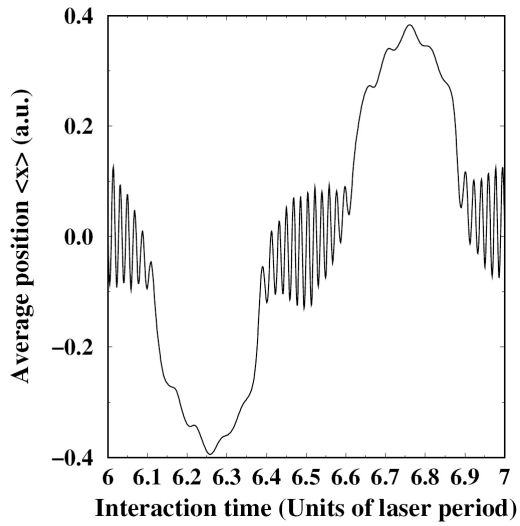

Figure 5. The average position $\langle x \rangle$ of the bound electronic wavepacket along the laser-polarization direction (x axis) as a function of the interaction time. The driving electric field (2) is sinusoidal in time. The parameters are the same as in Figure 4, but the calculation is for a small box in order to eliminate the effect of the ionized part of the wavefunction.

In Figure 5 we plot the expectation value $\langle x \rangle$ of the electronic wavepacket, which is obtained by using such a small box that the contribution from the tunneling part of the wavepacket is excluded. The large-scale sinusoidal structure of $\langle x \rangle$ reflects the motion of the minimum of the effective binding potential,

$$V_{\text{eff}}(x, t) = V(x, 0) + xE(t), \tag{12}$$

as a function of the laser field. The little wiggles visible in Figure 5 at those times when $\langle x \rangle$ goes through zero are related to the emission of the nontunneling harmonics (see below). A very crude time–frequency analysis can be performed by visual inspection of Figure 5, determining the frequency by counting the number of small wiggles within the time interval $6.4T$ –$6.6T$, where T is the laser period. This yields a harmonic order of about 60, which agrees very well with the cut-off position of Figure 4.

In Figure 6, we display the outcome for selected harmonics of a time–frequency analysis [28] of the electron acceleration $a_x(t) = \langle \ddot{x}(t) \rangle$ according to

$$a_x(t, \omega) = \int \mathrm{d}t'\, a_x(t') \mathrm{e}^{-\mathrm{i}\omega t'} \exp\left[-\frac{(t - t')^2}{\Delta t} \right], \tag{13}$$

with a time window of $\Delta t = 0.05T$, where T is the laser period and where $\langle \ddot{x}(t) \rangle$ is the expectation value of the acceleration operator for the time-dependent wavepacket. It shows that the harmonics within the plateau (H53 and H61) are emitted at two times during one optical cycle, around those times when the electric field goes through zero (recall from equation (2) that our field is proportional to sin ωt (since $z \cong 0$)). Remarkably, for H61 we observe two peaks near each of those times, which is reminiscent of the emission times of the long and the short trajectories of the Lewenstein model [14]. In contrast, the harmonic H29, which is situated at the low end of the plateau, is emitted at times when the field is definitely nonzero.

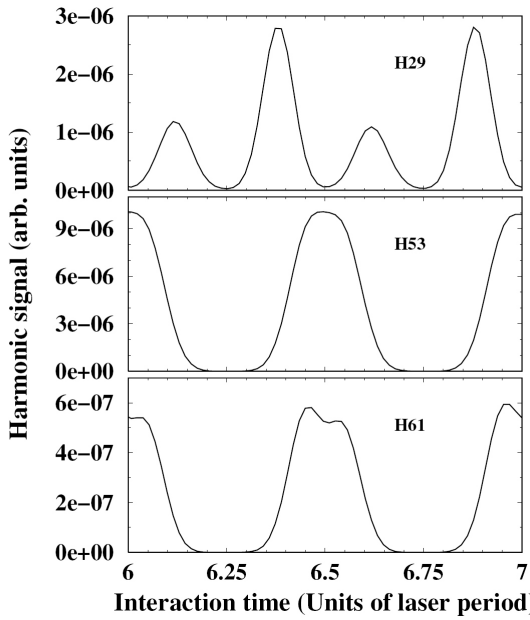

Figure 6. Plot of the absolute square of the electron acceleration $a_x(t, \omega)$ (cf. equation (13)) versus t for $6 \le t \le 7$ in units of the laser period T. The harmonic signal is proportional to the time integration of $|a_x(t, \omega)|^2$. Results are shown for three of the harmonics appearing in Figure 4: the 29th (upper panel), 53rd (middle panel) and 61st (lower panel).

3.2. A classical "surfing" mechanism for the nontunneling plateau

The nontunneling harmonics are amenable to a classical model description [17]. In order to justify the use of such a model, we notice that in Figure 1 there are several energy levels in the energy range in question. The effective potential (12) has a saddle point $x_s(t)$ given by $\partial V_{\text{eff}}(x, t)/\partial x|_{x_s} = 0$. This is a saddle point in two dimensions. In our classical modeling, we shall restrict ourselves to one dimension (x, which is the polarization direction of the laser field). Then, for the one-dimensional effective potential (12), the saddle point is a maximum as a function of x. Classically, electrons released with zero velocity inside this saddle point will tumble into the minimum of the effective potential, while those set free outside will move away from it. When the field decreases from its maximum to zero, the saddle point moves outward, and eventually reaches infinity. Figure 7 displays the position and the total-energy gain $\Delta\mathcal{E}_{\text{tot}}(t) = \mathcal{E}_{\text{tot}}(t) - \mathcal{E}_{\text{tot}}(t_0)$, where $\mathcal{E}_{\text{tot}}(t) = V_{\text{eff}}(x(t), t) + v_x(t)^2/2$ of an electron set free with zero velocity at the time $\omega t_0 = \pi/2$ at a position just outside the saddle point $x_s(t)$ when the electric field $E(t) = E \sin \omega t$ of the laser is at its maximum (and the saddle point is closest to the minimum of $V(x, 0)$). The precise value of the starting position was chosen as the maximal position that does not lead to immediate ionization. With ongoing time and decreasing field, the saddle point slowly moves outward and the electron moves with it, owing to the small outward-directed gradient of the effective potential. While the electron moves, riding on the saddle just outside its maximum, it gains energy from the laser field as the effective potential increases. As the field decreases further, the outward motion of the saddle point accelerates while the net outward force on the electron decreases. At some point in time (to be denoted by t_1 which is $\approx 0.42T$ in the figure), the electron cannot keep up any more and is drawn into the attractive region of the effective potential, where

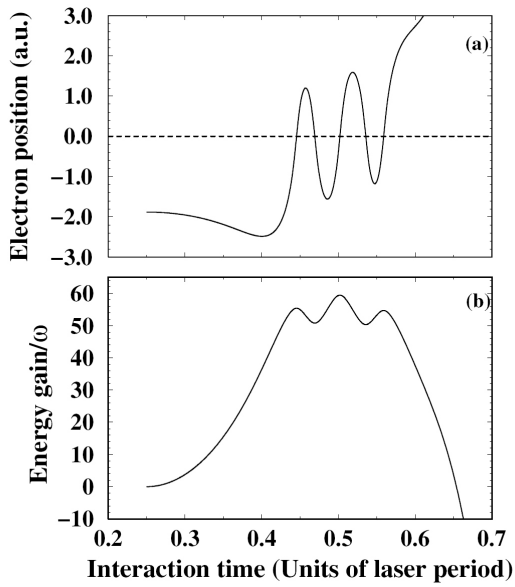

Figure 7. Position (*a*) and total energy gain (*b*) of a classical electron as a function of time for the conditions of Figure 4 with initial conditions as described in the text: namely, the electron starts just outside the saddle point of the effective potential (12) at a time when the field is maximal.

it oscillates back and forth a few times before it escapes from the binding potential when the field increases into its next half cycle. All of this is summarized in Figure 8. While the electron stays near the saddle point, its energy gain is about $\Delta\mathcal{E}_{\text{tot}} \approx V_{\text{eff}}(x_s(t_1)) - V_{\text{eff}}(x_s(t_0))$. This is the dominant part of its energy gain, but an additional smaller part is added during its ensuing oscillatory motion. Figure 7(*b*) shows that this mechanism is able to explain the cutoff predicted by the quantum mechanical calculation underlying Figure 4. Comparing Figure 7 with Figure 6, we can convince ourselves that the harmonics of the plateau (e.g. H53 and H61) are indeed emitted when the laser field is near zero and the electron orbit oscillates within the binding potential, unlike the lower harmonic H29. Figure 9 shows the results of an identical calculation, except that we have set the electron free just *inside* the saddle point. Now it remains confined to the attractive region of the effective potential. Its energy gain is much lower and remains well below the cutoff energy for all times.

The classical mechanism described above is the same by which a surfer first gains potential energy and then converts it into kinetic energy. Here, the electron surfs on the time-dependent effective potential (12). In a beautiful early above-threshold ionization (ATI) experiment [29], the electron was observed to surf on the time-dependent ponderomotive potential (whose time dependence is related to the envelope of the pulse).

A cutoff law of the form xE is reminiscent of the low-energy cutoff (in addition to the standard tunneling–recollision cutoff) observed in calculations of harmonic generation in a diatomic molecule having a pair of charge-resonant states [30, 31]. In the latter case, the electron gains energy by traveling the distance Δx from one atom to the other while the laser field is essentially constant. In the present case, the electron rides up in energy when the laser field decreases by ΔE while it essentially maintains its position x in space. The classical mechanism identified above depends very sensitively on the parameters. It is efficient if and only if the field-free ground-state energy $-I_p$ rather closely agrees with the energy $V_{\text{eff}}(x_s(t_0), t_0)$ of the saddle for

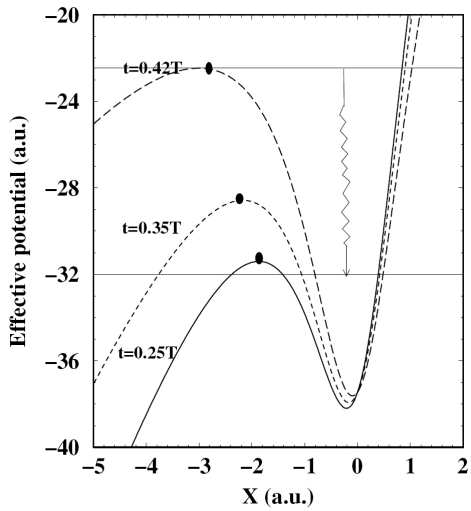

Figure 8. Illustration of the surfing mechanism described in the text. The effective potential (12) is plotted for the parameters of Figure 4 at three different times. The time $t = 0.25T$ corresponds to the maximum of the field. The solid dots represent the positions as a function of time of an electron that is released with zero velocity just outside the effective potential saddle at the time $t = 0.25T$, whose orbit is depicted in Figure 7. Notice how from $t = 0.25T = t_0$ to $t = 0.42T = t_1$ the electron moves from just outside to just inside the saddle point.

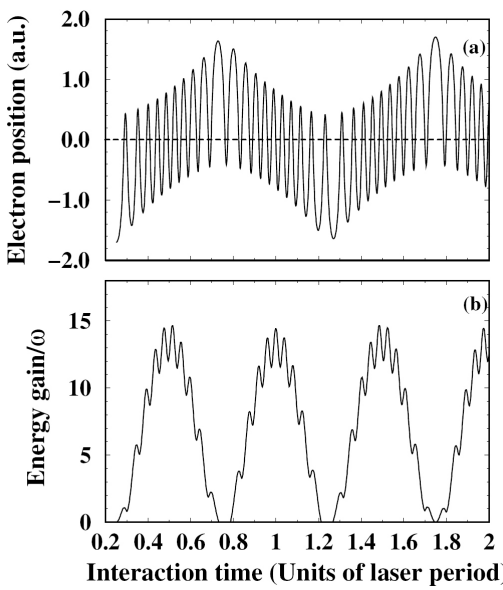

Figure 9. The same as Figure 7, but with the electron starting inside the saddle point.

t_0 near the maximum of the field. If it is much higher, the ion quickly undergoes further ionization; if it is lower, then the ground-state population at the position of the saddle is too small. For the case of Figure 4, when the field is maximal, the energy of the saddle point is $V_{\text{eff}}(x_s, t_0) = -31.4$ au, which is very close to the binding energy

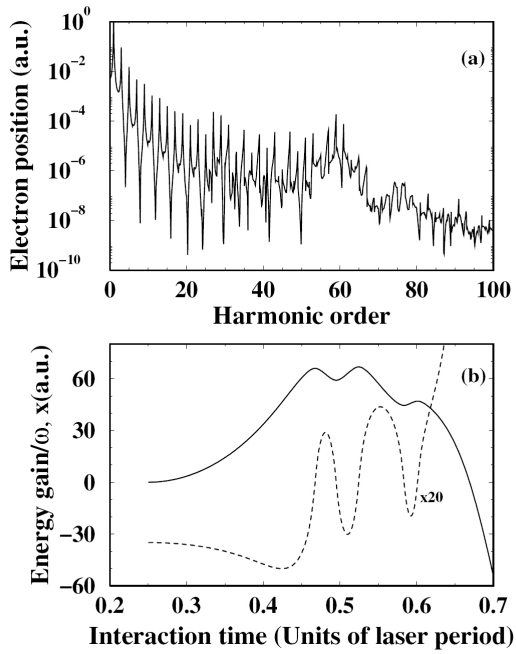

Figure 10. Harmonic spectrum (***a***) for the soft-core potential (7) with $k = 28$ and $q_e = 0.5$ and the result (***b***) of the same classical model as used in Figure 7. In (*b*), the dashed curve and the solid curve specify the position of the electron and its total-energy gain, respectively.

of −32 au. In order to explore this further, we decrease both the soft-core parameter k and q_e while keeping the ground-state energy fixed at −32 au. For $k = 28$ and $q_e = 0.5$, the resulting nontunneling harmonic spectrum is displayed in Figure 10, along with the orbit calculated from the same classical model. The spectrum is close to the one obtained above, but the efficiency of the plateau harmonics has decreased by about two orders of magnitude. This is primarily due to the fact that now the energy of the saddle point for maximal field is $V_{\text{eff}}(x_s, t_0) = -27.7$ au, which is far above the ground-state energy (but still far below the first excited state). Nevertheless, the classical model still correctly predicts the cutoff of the remainder of the plateau. This is particularly remarkable since now, according to Figure 1, the level density is quite low. We also note that, while the spectrum is still dominated by the odd harmonics of the laser frequency, for orders larger than 25 additional structure is showing up that was virtually absent from the spectrum of Figure 4.

3.3. Harmonic emission involving excited states

When we continue to decrease the soft-core parameters k and q_e, the spectral features of the harmonic emission change dramatically. In the upper panel of Figure 11 we plot the harmonic spectrum for $k = 15.32$ and $q_e = 0.1$, which corresponds to the potential depicted by the short-dashed curve in Figure 1. The plateau of the nontunneling harmonics is no longer the dominant feature of the spectrum. Rather, we observe a continuous decrease over six orders of magnitude from the lowest harmonics up to harmonic orders around 30. This part of the spectrum consists exclusively of odd harmonics of the laser frequency. There follows a resonance-like hump centered at an order just below 60. Above the order of 40, the odd harmonics have all but disappeared. In their place, we observe two series of harmonics: one having

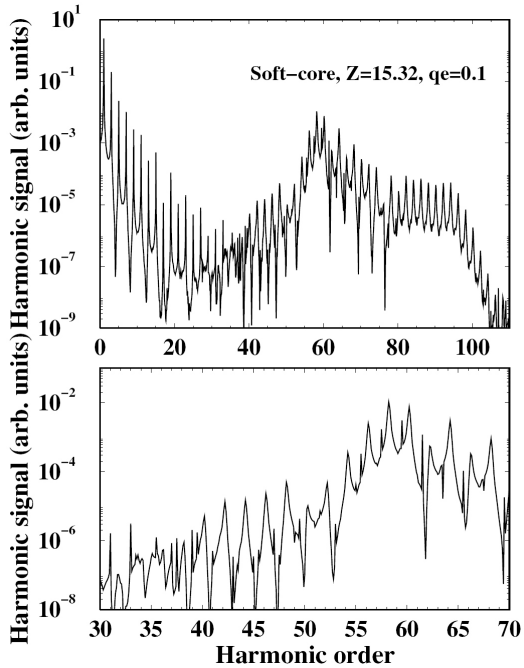

Figure 11. Harmonic spectrum for the soft-core potential (7) with k = 15.32 and q_e = 0.1. The lower panel shows a blow-up of the central part of the spectrum. It illuminates the transition from the purely odd harmonics of the low-energy part of the spectrum to the two series of harmonics characteristic of the upper part. The laser parameters are the same as those of Figure 4.

broad spikes at energies approximately equal to $(2n + 0.2)\omega$, the other having very narrow spikes at about $(2n - 0.5)\omega$ that are less intense by one to two orders of magnitude. The lower panel of Figure 11 displays an enlargement of the central part of the spectrum, which illustrates these statements. Starting at $n \approx 80$, a new plateau appears which extends up to a very pronounced cutoff at $n = 95$. This latter plateau consists almost entirely of the first series of broad spikes mentioned above.

From Figure 1(*b*) we can infer that in the absence of the laser field the energy separation between the ground state and the first excited state of the soft-core potential corresponds to about the 62nd harmonic, while the resonance-like hump shown in Figure 11 has its maximum just below the order of 60. It is tempting to associate the harmonics of the hump region with the transition from the first excited state to the ground state modulo an even number of photons (since the two states have opposite parity), so that their energies are given by $\hbar\omega_q = [E_e(I) - E_g(I)] + 2n\omega$ where E_e and E_g denote the energies of the ground state and the first excited state and I denotes the laser intensity. In this formula, we have allowed for dc Stark shifts of both the ground state and the excited state. While the Stark shift of the ground state is small, the excited state moves down substantially in energy, and this may explain the discrepancy between the field-free position of the resonance and the observed one. The second less intense series may be due to magnetic-dipole transitions from the excited state to the ground state modulo an odd-integer number of photons (owing to the positive parity of the magnetic-dipole transition). Each of these aspects requires further investigation; we discuss some of them further below.

The additional plateau above the hump, at harmonic orders between 75 and 95, is due to the classical "surfing" mechanism discussed in the preceding subsection.

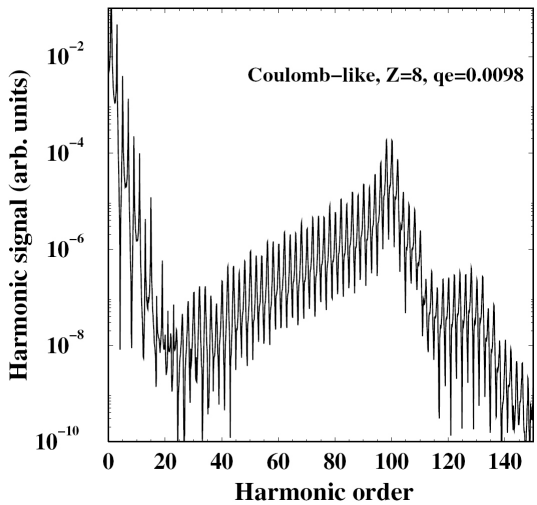

Figure 12. Harmonic spectrum for the soft-core potential (7) in the Coulombic limit, for $k = 8$ and $q_e = 0.0098$. The laser parameters are those of Figure 4.

The energy of the saddle point of the effective potential for maximal field is now $V_{\text{eff}} = -21$ au, which is very close to the energy of the first excited field-free state, −20.4 au (cf. Figure 1(*b*)). Hence, an electron promoted into this excited state has an excellent chance to experience the energy-gain mechanism described above, with the only difference being that now it starts from the excited state. Its maximal energy gain is about 35 harmonic orders. Hence, assuming it makes a radiative transition back to the ground state, we obtain a cutoff near $n = 95$, in good agreement with the spectrum of Figure 11.

We now decrease the parameter k further and adjust it to the charge of the ion O^{7+}, i.e. $k = Z = 8$. As discussed earlier, for hydrogen-like ions the parameter q_e is $q_e = q_e(\text{H})/Z^2$, where $q_e(\text{H}) = 0.63$; hence we obtain $q_e = 0.0098$. The corresponding potential is now very close to Coulombic (cf. the long-dashed curve in Figure 1(*a*)) and the first excited state is now at an energy of about 110 laser photons above the ground state. The resulting harmonic spectrum is shown in Figure 12. It exhibits a well developed resonant maximum at the harmonic order 99, which is, as was the case in Figure 11, below the order corresponding to the field-free excitation energy. The dc Stark shift is considerable because the first excited state comes close to being unbound in this case. We have calculated the dc-Stark-shifted energy levels for the peak laser field. This gives an energy of 94.8 ω for the transition between the first excited state and the ground state. The remaining difference between the quantum mechanically predicted resonance at 99 ω and the dc-Stark-shifted transition energy from the first excited state to the ground state (i.e. 94.8 ω) may be explained by the ac-Stark effect. Our quantum calculations of course include all effects; to interpret the results we have only calculated separately the dc-Stark shift.

In order to investigate the relation between the energy position of the resonance and the dc Stark shift, we have carried out similar calculations for three lower intensities, namely 10^{17}, 5×10^{17}, and 10^{18} Wcm^{-2}. The resulting harmonic spectra are presented in Figure 13. For the lowest intensity of 10^{17} W cm^{-2}, we observe a resonant maximum at the nominal field-free position, which can be read off from Figure 1(*a*). In fact, Figure 13(*a*) shows not only the resonance corresponding to the transition from the first excited state to the ground state, but also those from the second excited state to both the ground state (at about ~129.9 ω) and the first excited state

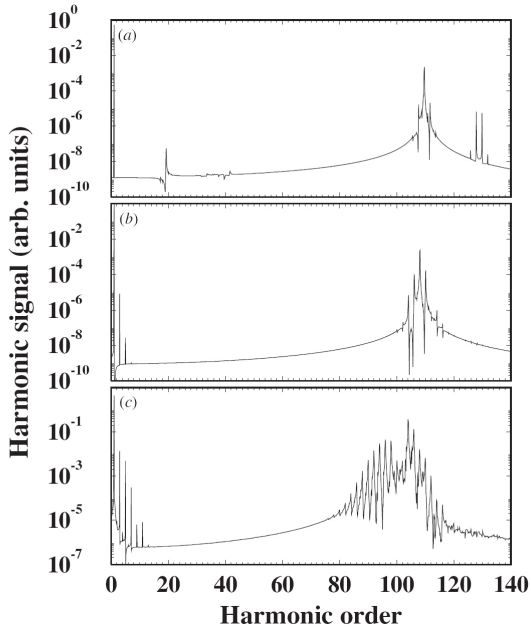

Figure 13. Harmonic spectra for the same Coulombic soft-core potential as for Figure 12 (cf. Figure 1(*a*)). The laser wavelength is 248 nm and the intensities are (*a*) 10^{17} W cm^{-2}, (*b*) 5×10^{17} W cm^{-2} and (*c*) 10^{18} W cm^{-2}.

(at about 19.3 ω). With increasing intensity, the excited-state–ground-state resonance moves to lower harmonic orders. At the same time, the effect of the second excited state is no longer visible, since for the higher intensities this state is above the classical barrier and ionizes very quickly. It is remarkable, too, that the lowest intensity is not yet capable of producing any low-order harmonics, owing to the electron being so strongly bound.

The harmonic spectra of Figure 11 and, in particular, of Figure 13 are reminiscent of spectra generated by atoms that have been prepared in a coherent superposition of the ground state and an excited state [32]. In contrast, here the atom is initially in the ground state and the superposition state is generated by the field-driven inner atomic dynamics.

Returning to Figure 12, we again observe a high-energy plateau above the resonance hump for orders between 110 and 135, with an appearance similar to that in Figure 11(*a*). Again we can invoke the classical mechanism, which predicts a maximal energy gain of 40 ω, starting from the saddle-point energy of $V_{\text{eff}}(x_s, t_0) = -15.30$ au, i.e. 16.7 au (or 91 ω) above the ground state. This yields a cutoff energy of 131 ω, which is remarkably close to that of the calculated spectrum shown in Figure 12. However, in comparison with Figure 11(*a*) the intensity of this plateau is low. This is not surprising: the energy of the field-free first excited state is now −11.9 au, which is high above the energy of the saddle point. The classical calculation already gives a hint regarding the reason for this low efficiency: the starting position of the electron must be chosen within an extremely narrow range in order to prevent immediate ionization.

Summarizing the dependence of the harmonic spectrum on the width of the soft-core potential, we have found that the density of the eigenstates and their positions relative to the height of the saddle appear to be most significant. The soft-core potential (7) with a large smoothing parameter q_e is comparatively broader and has a comparatively higher density of states than such potentials for small q_e. It gives rise

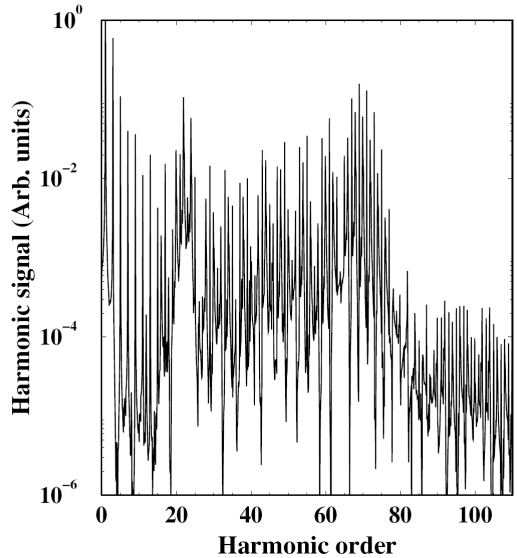

Figure 14. Harmonic spectrum for the approximate square-well potential (8) with Z = 12.95 and s = 2, depicted in Figure 2(*a*). The laser parameters are the same as those of Figure 4.

to a harmonic spectrum with a plateau that looks intriguingly similar to that of the usual tunneling–recombination harmonics. However, its cutoff can be understood classically by the surfing mechanism discussed above and not by the tunneling–recombination model. As is the case for the high-order harmonics produced by neutral atoms, there is little signature in the spectrum of particular excited states [33]. In contrast, as the smoothing parameter q_e in the potential (7) decreases, the density of states decreases, and resonance-like effects show up in the spectrum. These are due to electronic transitions from laser-populated excited states back to the ground state. In addition, the classical "surfing" plateau still exists for potentials with small values of q_e for high harmonic energies. In this case, the classical mechanism starts its action on an electron that has already been promoted by the field into an excited state. The efficiency depends upon how close the energy of the excited state is to the energy of the saddle point of the effective potential (12).

3.4. Square-well potential and two-level system

In this subsection we investigate binding potentials that have an extended almost flat part and, as a consequence, a high density of energy levels. In Figure 14 we display the gross structure of the harmonic spectrum of the approximate square-well potential (8) with Z = 12.95 and s = 2, whose energy levels are shown in Figure 2(*a*). The laser pulse is the same as for Figure 4. We notice first of all the presence of a very intense plateau quite similar to those of the soft-core potentials (shown in Figures 4 and 10). In order to investigate this spectrum in detail, we divide it into four parts, which are shown on an enlarged scale in Figure 15. The first few harmonics are exclusively odd harmonics of the laser frequency, as was the case for the soft-core potential (cf. Figure 10). However, in contrast to the former, here the odd harmonics survive throughout the entire spectrum in the form of narrow, sharply defined peaks. Very occasionally these odd harmonics are strongly suppressed (e.g. for n = 83). This points to the presence of several competing channels, which can give rise to a destructive interference, especially in the case where just two such channels are dominant. Starting with harmonic orders of about 12, two additional se-

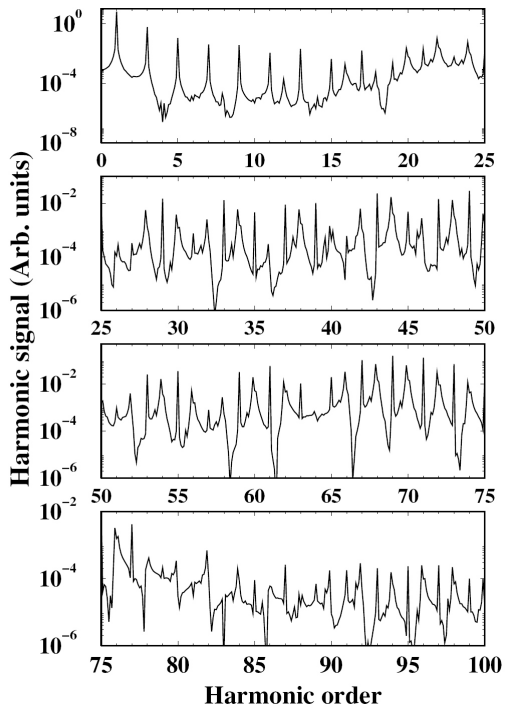

Figure 15. The same as Figure 14, but presented on an enlarged scale in order to display the details of the spectrum.

ries appear: one series consists of broad spikes centered at $(2n - 0.1)\omega$. These peaks clearly dominate the spectrum except for the very low harmonics. The second series is just barely visible, but consistently present. It manifests itself by narrow spikes at $(2n-0.5)\omega$, which ride on the low-energy shoulders of the first series.

If we change the parameters of our approximate square well to $Z = 10.7$ and $s = 10$ (cf. Figure 2(*b*)), its bottom becomes virtually flat. The harmonic spectrum for this potential is presented in Figure 16, for the slightly lower intensity of 1.2×10^{18} W cm^{-2}. The most important observation is that the plateau has disappeared. Moreover, except for the lowest few harmonics, there is no simple harmonic structure or, equivalently, there are many competing harmonic series. Obviously, this is due to the large extent of the binding potential, the associated high density of energy levels and the absence of a well defined potential minimum, about which a classical electron undergoes acceleration.

Finally, we consider the much investigated case of harmonics generated by a two-level system [34–37]. However, in contrast to previous work, we choose parameters such that the level separation corresponds to a large number of photons. Specifically, we use an energy separation of $\omega_0 = 3.068$ au, corresponding to the difference between the ground state and the first excited state of the square-well potential whose harmonic spectrum is shown in Figure 14. For the Rabi frequency we take $\Omega_0 = 7.348$ au. In view of its definition (10), this corresponds to the same laser electric field as for the previous figures, provided the electric-dipole transition matrix element has a value of one atomic unit. The resulting harmonic spectrum can be inspected in Figure 17. Its features conform with expectations: the cutoff agrees very well with the cutoff law [36], $\omega_{max} = 2[(\omega_0/2)^2 + \Omega_0^2]^{1/2} = 81.6\omega$. Throughout its range, the spectrum

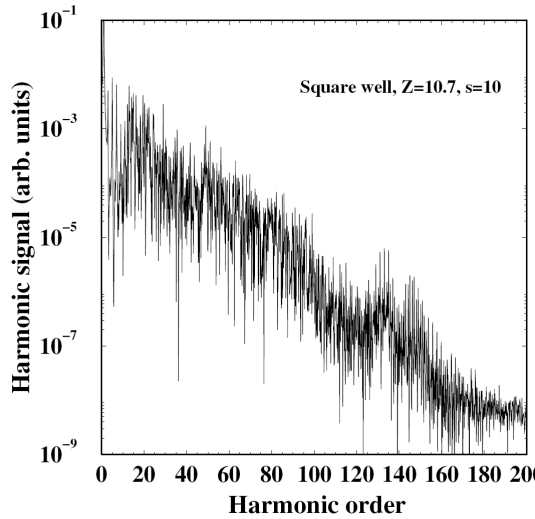

Figure 16. The same as Figure 14 but for $Z = 10.7$ and $s = 10$, corresponding to the potential of Figure 2(*b*), for a laser intensity of 1.2×10^{18} W cm^{-2}.

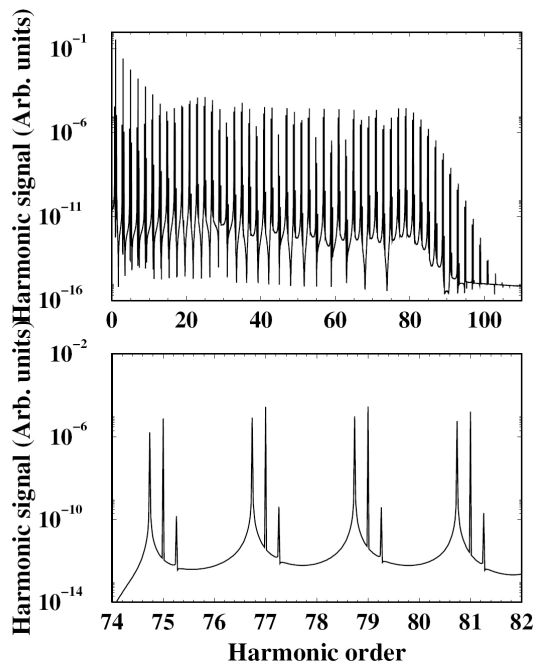

Figure 17. Harmonic spectrum of the laser-driven two-level atom described by (9) with $\omega_0 = 3.068$ au (corresponding to the energy separation between the ground state and the first excited state of the potential used for Figure 14) and $\Omega_0 = 7.348$ au. The lower panel shows part of the spectrum on a larger scale.

consists of triplets [35] that include a center frequency at odd harmonics of the laser frequency and two side bands positioned symmetrically at $(2n + 1 \pm 0.27)\omega$ on either side. The intensities of the side bands are, however, very asymmetrical. Except for

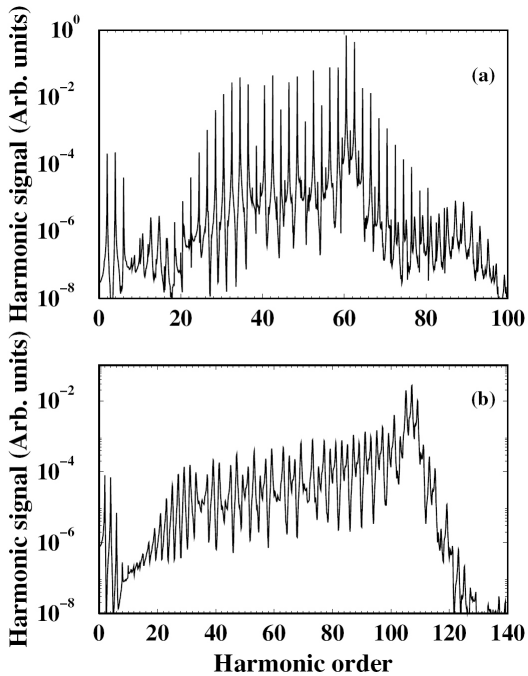

Figure 18. (*a*) Spectra of harmonics polarized in the *z* direction for the soft-core potential whose *x*-polarized spectrum is shown in Figure 11. (*b*) The same as in (*a*) but for the soft-core potential whose *x*-polarized harmonic spectrum is shown in Figure 12. The scale of the abscissa is different from those for the *x*-polarized spectra.

the lowest few harmonics, the high-energy side band has an intensity that is lower by four to five orders of magnitude than the one on the low-energy side. The reason becomes clear from the analyses in [35, 37]: actually, a triplet is composed of a $(2n + 1)\omega$ odd harmonic and two hyper-Raman lines, located at $2k\omega \pm \Omega$, where k is an integer, $-\infty \leq k \leq \infty$. Here, $\Omega \sim \Omega_0$ is much larger than the laser frequency ω. Hence the apparent hyper-Raman lines of a given triplet in Figure 17 originate from different integers k (namely, the triplets correspond to $2k\omega - \Omega$ and $2k'\omega + \Omega$). Thus these lines have very different intensities [37]. As noted above, our numerically predicted cutoff position agrees well with the analytic cutoff law of [36]; we find that it is numerically close also to the slightly different cutoff law of [37].

The two-level spectrum bears some resemblance to the spectrum of the square well shown in Figure 14, which also consists of triplets. However, the square-well-potential spectrum is much more irregular, and the sidebands are not symmetrical relative to the positions of the odd harmonics.

3.5. Significance of relativistic effects

The first relativistic effects that appear are related to the presence of the magnetic field or, equivalently, to the fact that the laser field is a propagating plane wave which depends on $t - z/c$ (cf. equation (2)) rather than just on t, as is assumed in the dipole approximation. As a result, the electron undergoes acceleration in the z direction, and there is harmonic radiation polarized in this direction which is absent if the dipole approximation is adopted. However, z-polarized radiation can also be emitted in the context of the dipole approximation, owing to spontaneous emission

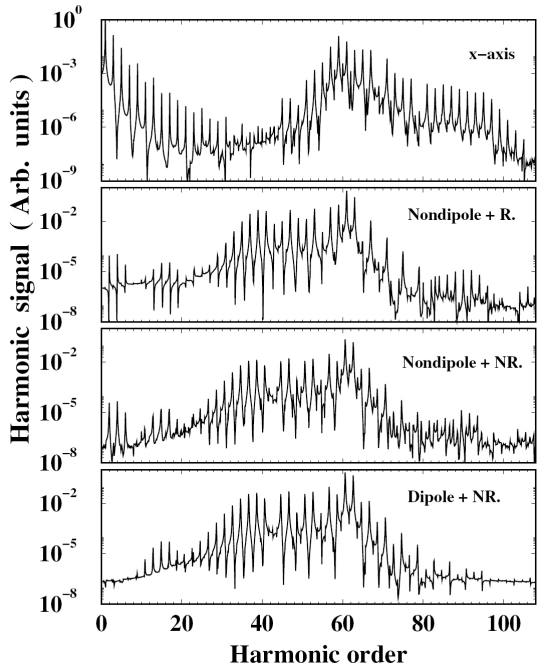

Figure 19. Testing retardation and relativistic effects via the harmonic spectrum polarized in the z direction: the potential is the soft-core potential ($k = 15.32$, $q_e = 0.1$) of Figure 11, with the slightly lower laser intensity of 1.7×10^{18} W cm^{-2}. The other laser parameters are the same as in Figure 4. The upper two panels show the x-polarized and the z-polarized spectra, respectively, calculated with the Hamiltonian (1). The x-polarized spectrum is virtually identical to that in Figure 11. In the next panel, the relativistic terms in the Hamiltonian (1) have been dropped, and in the lowest panel, in addition, the dipole approximation has been introduced. All panels but the uppermost show z-polarized spectra.

from an excited state. Whatever its origin, z-polarized radiation is calculated by Fourier transformation of the z-direction acceleration of the electron. In Figures 18(*a*) and (*b*) we show the harmonic spectrum polarized in the z direction for the two soft-core potential cases whose x-polarized harmonic spectra were presented in Figures 11 and 12.

Both z-polarized spectra exhibit a strong suppression of the low-order harmonics, which are practically absent save for the very lowest even harmonics. These latter are due to even-parity magnetic-dipole emission. The resonance-related parts of the spectra differ from the x-polarized spectra in two respects. First, the z-polarized spectra peak precisely at the field-free excitation energies. There is no evidence of a dc Stark shift. Second, the plateaux on the high-energy shoulders of the x-polarized spectra appear on the low-energy shoulders of the z-polarized spectra and are broader.

Finally, in Figure 19 we investigate the extent to which the z-polarized spectra are related to relativistic effects. We do this by first omitting the first-order relativistic term in the Hamiltonian (1) and then by introducing, in addition, the dipole approximation in the remaining NR Hamiltonian. The results show that the first-order relativistic term has virtually no effect on the spectrum, except for the highest harmonics in the spectral region where the x-polarized spectrum displays its plateau. The dipole approximation, on the other hand, markedly affects the spectrum in two ways (cf. the lower panel of Figure 19): first, the low even harmonics completely dis-

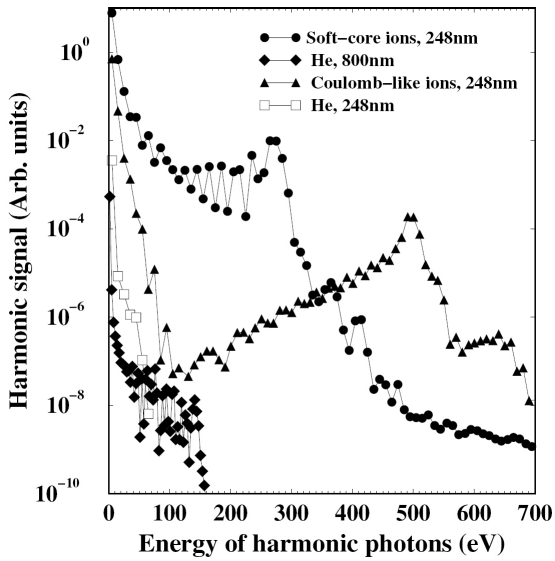

Figure 20. Comparison of the harmonic spectrum of Figure 4 (filled circles) with a standard (tunneling–recombination) harmonic spectrum in neutral helium for the same wavelength (λ = 248 nm) (open squares) as well as for the longer wavelength of 800 nm (filled diamonds), the latter two at intensities near saturation, 10^{15} W cm^{-2} and 6×10^{14} W cm^{-2}, respectively. Also reproduced is the spectrum of Figure 12 (filled triangles). All spectra have been obtained by running the same code and are plotted on the same scale.

appear. This confirms that they are due to magnetic dipole emission. Second, the remainder of the plateau on the high-order shoulder of the resonance disappears. In contrast, the plateau on the low-energy side of the resonance is practically unaffected. This assures us that it is related to spontaneous field-assisted decay of the first excited state.

4. Conclusions

The high efficiency of the nontunneling harmonics discussed in this paper is due to the fact that they are generated by the field-induced motion of that part of the electronic wavepacket that stays inside the range of the binding potential. This is by far the dominant part, as opposed to the continuum part that has tunneled out and is responsible for the standard tunneling–recombination harmonics [5, 6, 14, 15]. In Figure 20 we compare the intensities of the standard harmonics generated by a neutral atom and the nontunneling harmonics generated by a multiply charged ion, with each exposed to an ultra-intense field having an intensity close to that leading to saturation. In the figure, we reproduce the results for the soft-core potential with $q_e = 1$ and $k = 37.45$ (Figure 4) and for the Coulomb-like potential with $q_e = 0.0098$ and $k = 8$ (Figure 12) (with both potentials having the same binding energy, which equals that of O^{7+}), and compare these with harmonic spectra calculated for helium near the saturation intensity. The plot was obtained by running the same code for all cases. The figure shows that the nontunneling harmonics are radiated with an intensity that is higher by about four orders of magnitude for the low orders (and, of course, more than that once the harmonic order is above the cutoff in the atomic case). This very substantial harmonic yield may leave hope for an experimental observation, even though the density of an ion target will not be high.

On the theoretical side, the examples presented in this paper underline once again that the existence in the harmonic response of a plateau with a well defined cutoff is not tied to the tunneling–recombination mechanism. Rather, it is a very general phenomenon characteristic of nonlinear systems that are sufficiently strongly driven by a periodic force [38, 39]. Other examples include two-level systems [34, 35] and two-center systems [30, 31]. We feel there exists no explanation of the formation of this plateau that is as universal as the phenomenon itself.

The laser field that we employed is so intense that the free-electron motion in its presence is moderately relativistic. Yet, when in our calculations we disregard the relativistic correction and even introduce the dipole approximation, the harmonic spectra hardly change at all. A similar suppression of relativistic effects is known theoretically for ionization and for other processes induced by intense relativistic low-frequency fields: the total rates which are determined by the inner atomic dynamics display relativistic effects only reluctantly and for intensities that are much higher than those required to make strong marks on the differential rates with charged particles in the final state [40]; see also remarks in [41]. There is a recent experimental confirmation through a measurement of ionization of high-charge states of argon by relativistic fields [42]. Briefly, in order to accelerate to relativistic velocities, the electron needs more space than is available within the range of the binding potential. Also for an electron in a hydrogenic ion such as O^{7+}, which has the same binding energy as the potentials in this paper, even a laser of intensity 10^{18} W cm^{-2} has an electric field that is only 2% of that due to the nucleus. Hence since electronic motion about an O^{7+} nucleus may be treated nonrelativistically, one should not expect even a laser of 10^{18} W cm^{-2} intensity to introduce significant relativistic effects, unless of course the electron leaves the vicinity of the nucleus. The lack of significant relativistic effects in our calculations thus gives added confirmation of our nontunneling model interpretation of our results.

Acknowledgments

We enjoyed useful discussions with R. Kopold. S.X.H. and D.B.M. gratefully acknowledge support by the Alexander von Humboldt Foundation for part of the period when this work was carried out. D.B.M. also acknowledges partial support from the VolkswagenStiftung. S.X.H. and A.F.S. acknowledge partial support of the US National Science Foundation under grant no PHY- 0070980.

References

[1] Salières P, L'Huillier A, Antoine Ph, and Lewenstein M 1999 *Adv. At. Mol. Opt. Phys.* **41** 83

[2] Brabec T and Krausz F 2000 *Rev. Mod. Phys.* **72** 545

[3] Drescher M, Hentschel M, Kienberger R, Tempea G, Spielmann Ch, Reider G A, Corkum P B, and Krausz F 2001 *Science* **291** 1923

[4] Paul PM, Toma E S, Breger P, Mullot G, Augé F, Balcou Ph, Muller H G, and Agostini P 2001 *Science* **292** 1689

[5] Corkum P B 1993 *Phys. Rev. Lett.* **71** 1994

[6] Kulander K C, Schafer K J, and Krause J L 1993 *Super Intense Laser–Atom Physics* (*NATO ASI Ser. B vol 316*) ed. B Piraux, A L'Huillier, and K Rzążewski (New York: Plenum) p 95

[7] Gillaspy J D 2001 *J. Phys. B: At. Mol. Opt. Phys.* **34** R93

[8] Mokler P H and Stöhlker Th 1996 *Adv. At. Mol. Opt. Phys.* **37** 297; Ullrich J, Moshammer R, Dörner D, Jagutzki O, Mergel V, Schmidt-Böcking H, and Spielberger L 1997 *J. Phys. B: At. Mol. Opt. Phys.* **30** 2917; Snyder E M, Buzza S A, and Castleman A W Jr 1996 *Phys. Rev. Lett.* **77** 3347; Ditmire T, Tisch J W G, Springate E, Mason M B, Hay N, Marangos J P, and Hutchinson M H R 1997 *Phys. Rev. Lett.* **78** 2732

[9] For example, the GSI laboratory in Darmstadt is developing PHELIX (Petawatt High-Energy Laser for Heavy-Ion Experiments); online web page http://www.gsi.de/phelix

[10] West J B 2001 *J. Phys. B: At. Mol. Opt. Phys.* **34** R45

[11] Hatsagortsyan K Z and Keitel C H 2001 *Phys. Rev. Lett.* **86** 2277

[12] Perry M D and Mourou G 1994 *Science* **264** 917; Protopapas M, Keitel C H and Knight P L 1997 *Rep. Prog. Phys.* **60** 389

[13] Delone N B and Krainov V P 1998 *Usp. Fiz. Nauk* **168** 531 (Eng. transl. 1998 *Sov. Phys.–Usp.* **41** 469)

[14] Lewenstein M, Balcou Ph, Ivanov M Yu, L'Huillier A, and Corkum P B 1994 *Phys. Rev.* A **49** 2117

[15] Becker W, Long S, and McIver J K 1990 *Phys. Rev.* A **41** 4112; Becker W, Long S, and McIver J K 1994 *Phys. Rev.* A **50** 1540; Becker W, Lohr A, Kleber M, and Lewenstein M 1997 *Phys. Rev.* A **56** 645

[16] Hu S X and Xu Z Z 1997 *Phys. Rev.* A **56** 3916; Hu S X and Xu Z Z 1997 *Appl. Phys. Lett.* **71** 2605

[17] Hu S X, Milošević D B, Becker W, and Sandner W 2001 *Phys. Rev.* A **64** 013410

[18] Feit M D, Fleck J A Jr, and Steiger A 1982 *J. Comput. Phys.* **47** 412; Hermann M R and Fleck J A Jr 1988 *Phys. Rev.* A **38** 6000

[19] Krause J L, Schafer K J, and Kulander K C 1992 *Phys. Rev.* A **45** 4998

[20] Kulander K C, Schafer K J, and Krause J L 1992 *Atoms in Intense Laser Fields* ed. M Gavrila (New York: Academic) pp 247–300

[21] Reiss H R 2001 *Phys. Rev.* A **63** 013409

[22] Hu S X and Keitel C H 1999 *Phys. Rev. Lett.* **83** 4709

[23] Vázquez de Aldana J R and Roso L 2000 *Phys. Rev.* A **61** 043403

[24] Hu S X and Keitel C H 2001 *Phys. Rev.* A **63** 053402

[25] Eberly J H, Su Q, and Javanainen J 1989 *Phys. Rev. Lett.* **62** 881

[26] Milošević D B 2000 *J. Phys. B: At. Mol. Phys.* **33** 2479

[27] Milošević D B, Hu S X, and Becker W 2001 *Phys. Rev.* A **63** 013403(R)

[28] Rae S C, Burnett K, and Cooper J 1994 *Phys. Rev.* A **50** 3438; Antoine Ph, Piraux B, Milošević D B, and Gajda M 1996 *Phys. Rev.* A **54** R1761

[29] Bucksbaum P H, Freeman R R, Bashkansky M, and McIlrath T J 1987 *J. Opt. Soc. Am.* B **4** 760

[30] Ivanov M Yu and Corkum P B 1993 *Phys. Rev.* A **48** 580; Zuo T, Chelkowski S, and Bandrauk A D 1993 *Phys. Rev.* A **48** 3837

[31] Kopold R, Becker W, and Kleber M 1998 *Phys. Rev.* A **58** 4022

[32] Watson J B, Sanpera A, Chen X, and Burnett K 1996 *Phys. Rev.* A **53** R1962; Sanpera A, Watson J B, Lewenstein M, and Burnett K 1996 *Phys. Rev.* A **54** 4320

[33] Figueira de Morisson Faria C, Dörr M, and Sandner W 1998 *Phys. Rev.* A **58** 2990

[34] Sundaram B and Milonni P W 1990 *Phys. Rev.* A **41** 6571; Plaja L and Roso-Franco L 1992 *J. Opt. Soc. Am.* B **9** 2210; Kaplan A E and Shkolnikov P L 1994 *Phys. Rev.* A **49** 1275

[35] Gauthey F I, Keitel C H, Knight P L, and Maquet A 1995 *Phys. Rev.* A **52** 525; Gauthey F I, Keitel C H, Knight P L, and Maquet A 1997 *Phys. Rev.* A **55** 615

[36] Gauthey F I, Garraway B M, and Knight P L 1997 *Phys. Rev.* A **56** 3093

[37] Di Piazza A, Fiordilino E, and Mittleman M H 2001 *Phys. Rev.* A **64** 013414

[38] Leopold J G and Richards D 1993 *J. Phys. B: At. Mol. Opt. Phys.* **26** 1519

[39] Balcou Ph, L'Huillier A, and Escande D 1996 *Phys. Rev.* A **53** 3456

[40] Becker W, Schlicher R R, and Scully M O 1990 *Advances in Multi-Photon Processes and Spectroscopy* vol 6, ed. S H Lin (Singapore: World Scientific) p 110

[41] Taïeb R, Véniard V, and Maquet A 1998 *Phys. Rev. Lett.* **81** 2882; Taïeb R, Véniard V and Maquet A 2001 *Phys. Rev. Lett.* **87** 053002

[42] Chowdhury E A, Barty C P J, and Walker B C 2001 *Phys. Rev.* A **63** 042712